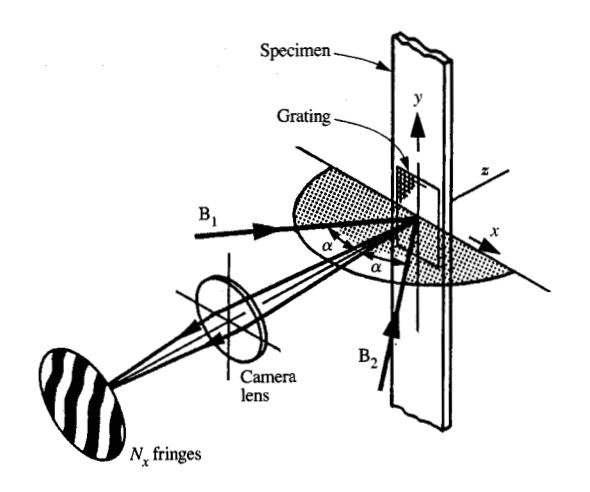
Solder Ball Connect (SBC) assemblies under thermal loading: I. Deformation measurement via moiré interferometry, and its interpretation

by Y. Guo C. K. Lim W. T. Chen C. G. Woychik

Thermal deformations that result from mismatches of coefficients of thermal expansion (CTE) in Solder Ball Connect (SBC) assemblies were investigated. The CTE mismatches of the materials and the components in the package have both macro and micro effects on the strain distributions in the SBC interconnections. The geometry of the SBC joint also has a strong influence on the solder strains in the SBC package. An

experimental technique with high sensitivity and resolution, moiré interferometry, was used to obtain whole-field displacements. Thermal strains in SBC packages, especially the strain concentrations in the SBC joints, were then determined from the displacement fields. The experimental results played an important role in failure analysis, structural design optimization, and finite element model verification in the IBM SBC program. The

<sup>e</sup>Copyright 1993 by International Business Machines Corporation. Copying in printed form for private use is permitted without payment of royalty provided that (1) each reproduction is done without alteration and (2) the *Journal* reference and IBM copyright notice are included on the first page. The title and abstract, but no other portions, of this paper may be copied or distributed royalty free without further permission by computer-based and other information-service systems. Permission to *republish* any other portion of this paper must be obtained from the Editor.



Principle of moiré interferometry. (From [7], reprinted with permission.)

results also show that moiré interferometry is a very powerful and effective tool in experimental studies of electronic packaging.

# Introduction

In Solder Ball Connect (SBC), an area array surface mount technology in which ceramic modules are connected to circuit boards by means of solder balls, thermal fatigue of the solder is a major factor in determining the reliability of the package. The fatigue life of the solder is usually a function of the magnitudes of the plastic and elastic strains [1, 2]. If those strains can be determined mathematically or actually measured experimentally, the fatigue life of the solder can be estimated. Many researchers have studied low-cycle fatigue of the solder and its relation to the solder strains [3-5]. It has been pointed out that the strain distributions in the solder joints are nonuniform. However, because of the difficulties of determining the strain concentrations in an already small joint, effective strains, such as average shear strain, have been used as parameters in models of the fatigue life of solder joints. If the effective strain used in such a model is close to the strain that actually causes fatigue damage, its use provides a good approximation. In many cases, especially in specially designed solder fatigue tests, the effective strain value does dominate the failure mechanism. However, if the strain variations are dramatic and the strain concentrations are significant, the fatigue damage is generally dependent upon the maximum strain instead

of the average strain. Therefore, when fatigue life is estimated, it is important to be aware of the strain distributions, the maximum strains and their locations, and thus the failure mechanism.

As electronic technology advances, solder joints used in electronic packaging are becoming smaller and smaller. The determination of strain distributions becomes more and more complicated. Packaging structures usually consist of several materials and interfaces, all with different mechanical properties, and strain concentrations are frequently localized in very tiny zones of the solder joints. Such situations make the measurement of strain distributions extremely difficult. In this paper, a highly sensitive optical technique, moiré interferometry, is applied to the analysis of displacement and strain in SBC packages. By means of this technique, strain concentrations in very localized areas in solder joints have been determined. The results show that the strains are nonuniformly distributed over the solder joints and that the maximum strains are much higher than the average strain values. It has been proven that this experimental technique is well suited to and has great potential for the mechanical study of electronic packaging.

The experimental analysis revealed that the thermal strains in the SBC joints are closely related to the coefficients of thermal expansion (CTE) of the materials used in the package. It was found that the strain concentrations are significant and that strain variations are dramatic in the solder joints. The strain concentrations and their locations are very sensitive to the geometries of the solder joints. Fatigue damage is due to the maximum strains.

### Experimental technique—moiré interferometry

Moiré interferometry is a whole-field optical technique for determining in-plane\* displacements and strains [6]. It features very high displacement sensitivity and spatial resolution. The principle of this technique is depicted schematically in Figure 1 [7]. With this method, a fine diffraction grating is placed on the specimen surface at the testing area. This specimen grating is usually a crossed-line grating with orthogonal grating lines. It can be fabricated by lithography or by simple replication from an existing grating. During experiments, the specimen grating deforms along with the specimen under an applied mechanical or thermal loading, so that the deformation of the grating represents the deformation of the specimen. The optical arrangement in a moiré interferometry system produces a virtual reference grating of spatial frequency f by means of the interference pattern of two coherent beams B, and B, (with plane wavefronts) from a laser light source. The frequency  $f[f = (2/\lambda) \sin \alpha]$  is a function of the

<sup>\*</sup>In this paper, "in-plane" refers to the geometric plane in which measurements are made.

wavelength  $\lambda$  of the laser light and the incident angle  $\alpha$  of the two coherent beams. The virtual reference grating is superimposed on the specimen grating, and the interaction of the two gratings forms a fringe pattern, which is a contour map, with each fringe passing through points with the same displacement U. Fringes are numbered consecutively, with fringe order  $N_x$ . The fringes are equivalent to geometric moiré fringes. In Figure 1, the two beams  $B_1$  and  $B_2$ , separated by angle  $2\alpha$  in the horizontal plane, produce the contour map of  $N_x$ . An additional two beams (not shown), separated by an angle in the vertical plane, produce the contour map of  $N_y$ .

In a fringe pattern, the fringe order N of a point is proportional to the displacement of the point. Usually, the fringe patterns of two perpendicular displacement fields U and V, corresponding to the x and y directions, respectively, are recorded at the same time. The equations for determining U and V displacements from the fringe orders can be written

$$U = \frac{N_x}{f}$$
 and  $V = \frac{N_y}{f}$ , (1)

where  $N_x$  and  $N_y$  are the fringe orders in the corresponding fringe patterns. Linear strains can be calculated by taking the derivatives of the displacements U and V, leading to

$$\epsilon_x = \frac{1}{f} \frac{\partial N_x}{\partial x}, \quad \epsilon_y = \frac{1}{f} \frac{\partial N_y}{\partial y}, \quad \epsilon_{xy} = \frac{1}{2f} \left( \frac{\partial N_x}{\partial y} + \frac{\partial N_y}{\partial x} \right).$$
 (2)

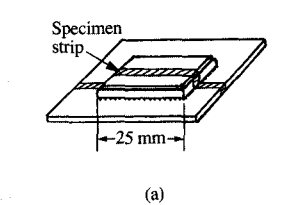
The linear strain values can also be obtained directly from the fringe patterns by measuring the fringe gradients.

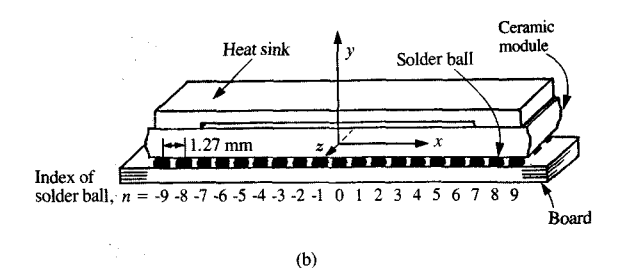
The typical displacement sensitivity of moiré interferometry is about 0.5  $\mu$ m per fringe order. Therefore, detailed strain distributions can be obtained in very small and localized areas. In this work, a reference grating f=2400 lines per mm is used, providing a displacement sensitivity of 417 nm per fringe order.

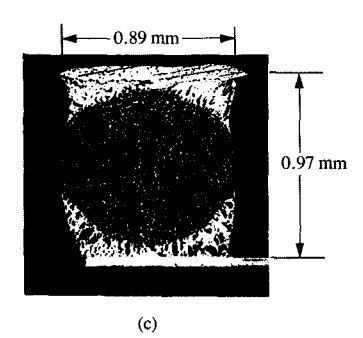
### Specimen and experimental procedure

The specimen used in the experiments described in this work was a strip cut from a 25-mm SBC assembly. Schematic diagrams of the assembly and the specimen are shown in Figures 2(a) and 2(b), together with a photograph of a cross section of an SBC joint in Figure 2(c). The cross section of the specimen was cut along a row of solder balls and contained cross sections of all 19 solder balls in the row. As shown in Figure 2(b), an index number n was used to identify the solder balls in the cross section. A strip specimen was used to ensure a two-dimensional deformation and to eliminate bending in the y-z plane.

The assembly is a second-level package in which a multilayer ceramic module is directly joined to a glass-epoxy printed circuit board by a  $19 \times 19$  solder ball array. The module has an average coefficient of thermal

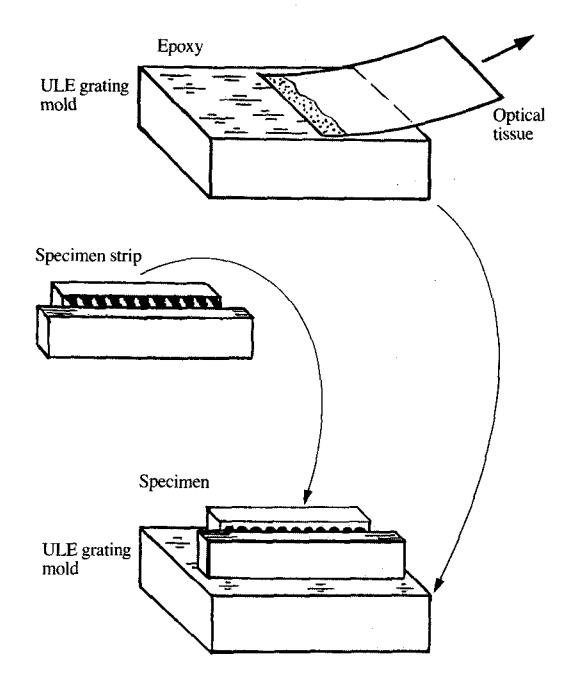






Specimen strip cut from SBC assembly: (a) SBC assembly; (b) specimen strip, providing cross section of assembly; (c) photograph of solder ball joint.

expansion of 6.5 ppm/°C and a thickness of 2.8 mm (110 mils). The board has an average CTE of 19 ppm/°C and a thickness of 1.5 mm (60 mils). On top of the module is an aluminum heat sink attached by epoxy adhesive. The SBC solder balls, used to join the module and the board, are made of solder with a high melting point; eutectic (low-melting-point) solder forms the solder fillets in the joints. The solder balls are 0.89 mm (35 mils) in diameter and are spaced 1.27 mm (50 mils) apart. After the joint is formed, the actual separation from the board to the module, or the height of the SBC joint, is 0.97 mm (38 mils). The pads used on the module side have diameters of 0.86 mm (34 mils) and on the board side, 0.71 mm (28 mils). The contact areas of the solder joints to the module and the board are determined by the pad sizes.



Procedure for applying the specimen grating (in an oven at elevated temperature).

The thermal loading that caused the measured deformations was applied by cooling the specimen from an elevated temperature  $T_1$  to room temperature  $T_2$ . The grating was placed on the specimen while the specimen was held at elevated temperature  $T_1$ , and the measurements were conducted at temperature  $T_2$ . Thus, the deformations of the specimen grating reflect the deformations experienced by the specimen under thermal loading  $\Delta T$  ( $\Delta T = T_2 - T_1$ ).

The following steps were used to place a uniform grating of known frequency (undeformed grating) on the specimen at an elevated temperature [8, 9] (Figure 3): A ULE (Ultra Low Expansion) glass grating mold was first produced. Two aluminum coatings (to facilitate subsequent separation) were vacuum-evaporated on the grating mold, and a very thin layer of adhesive (epoxy) was used to attach the grating to the specimen in an oven with an elevated temperature. As shown in Figure 3, the thin layer of epoxy was applied to the grating mold by dragging an epoxy-wetted tissue across the grating surface. Because the epoxy had very low viscosity at the elevated temperature, a thin and uniform layer was formed. The specimen and the ULE grating were then pressed together

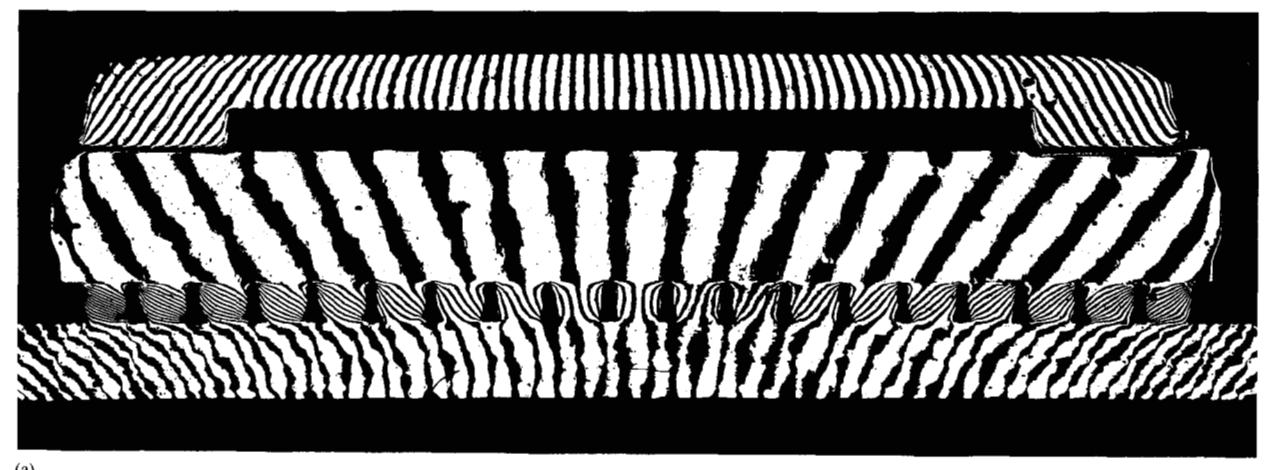
and maintained at the elevated temperature until the epoxy was cured. When the specimen was separated from the ULE grating mold, one of the aluminum coatings with the grating profile was transferred to the specimen surface. The specimen was cooled from 82°C to room temperature (22°C), and measurements were conducted. A very important factor in successfully producing specimen gratings is maintaining clean edges on the solder joints, since excessive adhesive reinforces the solder and changes local strain distributions.

The specimen was maintained at 82°C for about one hour before the specimen grating was applied. After being cooled to room temperature, the specimen was allowed to creep for one hour before the measurements were conducted. The dwell time was selected to allow the solder to creep fully and the plastic strains to develop fully. The use of dwell time also helped in achieving repeatability of the measurements.

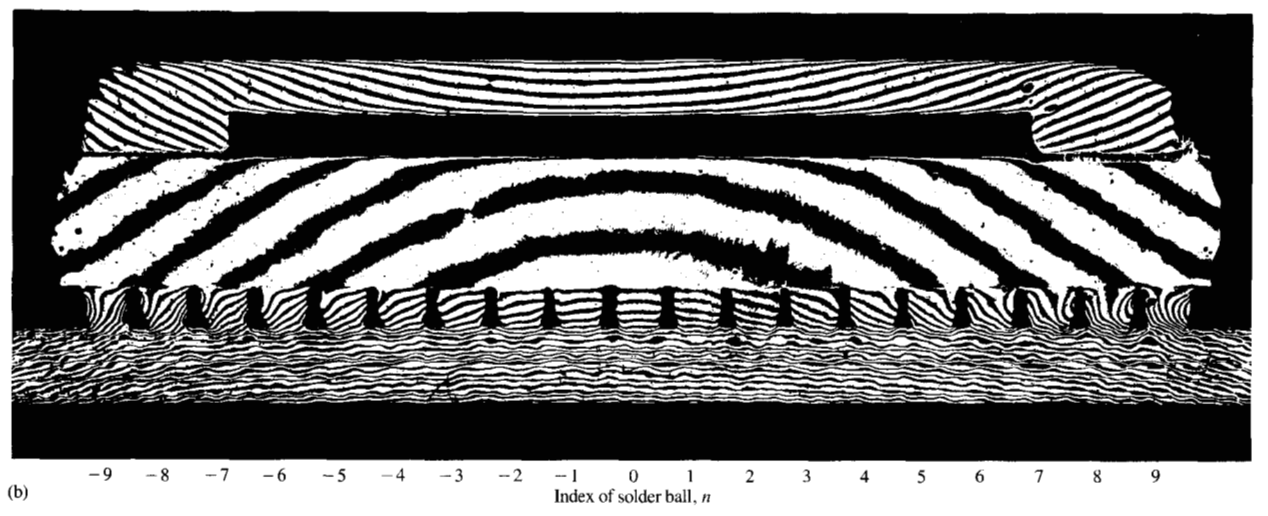
The moiré interferometry system was designed to obtain both U and V displacement fields. The frequency of the virtual reference grating was adjusted to match the frequency of the ULE grating (in both x and y directions) that was used to form the original specimen grating. This procedure is also called adjusting the null field, which zeroes the optical system and ensures that the fringes measured later are load-induced fringes. The specimen was held on a fixture that allowed rigid-body rotations when the measurements were conducted. By rotation of the specimen, the specimen grating was aligned with the virtual reference grating. Fringe patterns were then recorded.

Because the fringe patterns were recorded at room temperature, no environmental chamber was needed in the moiré interferometry system. The camera was focused directly on the specimen surface, so that high-spatial-resolution, good-quality photographs were achieved. The carrier fringe technique [7] was applied during the experiment.

Figure 4 shows typical fringe patterns of U and Vdisplacement fields obtained from an SBC specimen. After the specimen was cooled by 60°C, all of the components contracted in both the x and y directions. The deformations in the ceramic module are very small (indicated by the low fringe density), because the material has low CTE and high Young's modulus. In the printed circuit board, the y-direction contraction is much greater than the x-direction contraction (shown by the higher fringe gradient in the V-field fringe pattern) because of the anisotropic CTE property of the board. The board also bent, as one can see from the inclined fringes in the U displacement field. In the x direction, the CTE mismatch resulted in different displacements in the module and the board. Their relative displacement at any point is a function of the distance from that point to the geometric



(a)



Fringe patterns of the SBC cross section: (a) U displacement field; (b) V displacement field.

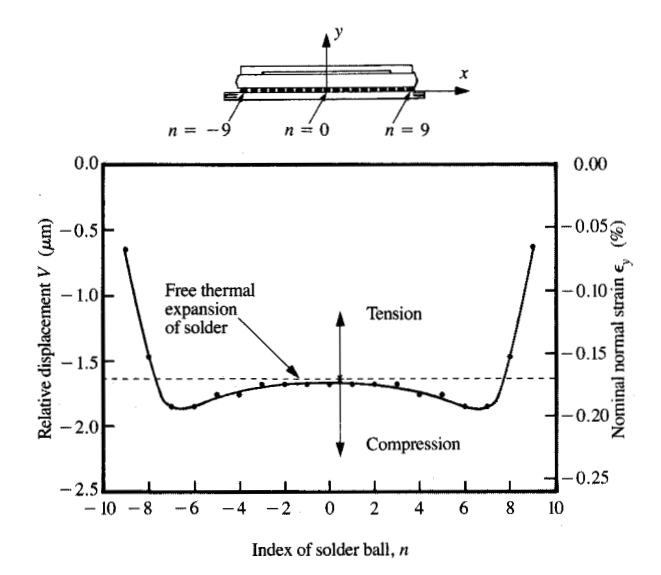
center of the assembly. At the ends of the module, the relative displacement reaches its maximum value, which causes the highest stress and strain in the rightmost and leftmost solder joints. The increase in fringe density in the solder joints with distance from the center is readily observed in Figure 4(a). The strains and their distributions in all 19 solder joints can be determined from the fringe patterns.

### Results and analysis

Because of the complexity of the thermal deformation in the SBC package, the analysis is divided into two steps, one related to macro (or global) deformations and the other to micro (or local) deformations. The macro step is used to describe the global deformations at the level of the entire SBC package; each solder joint is treated as an element with a nominal strain value (average strain along the vertical centerline of the joint). Macro deformation is due to the mismatch between the CTEs of the module and the board. (This CTE mismatch is called "macro CTE mismatch" in this paper.) The impact of the macro deformation upon the solder joints is referred to as the macro effect.

In micro deformation, the local deformations in the individual solder joints are studied. (The CTE mismatches at the interfaces of solder ball to module and solder ball to board are called "micro CTE mismatches.") The impact on solder strains caused by the micro CTE mismatches and by the local forces at the interfaces is referred to as the micro effect. Because the solder joints interface with components (module and board) that have mechanical properties very different from those of the solder, the

639



Relative displacement between the module and the board in the y direction, and the resulting nominal normal strain in each solder joint.

strain variations near the interfaces are significant. Micro deformation describes the strain distributions and concentrations in the individual solder joints and near the interfaces.

• Macro deformations and nominal strains in solder joints In this section, the thermal deformations of the SBC structure and the resulting nominal strains in the solder joints are studied. The macro deformation is dictated by the macro CTE mismatch, and the resulting nominal strains in the solder joints are referred to as the macro effect.

### Macro normal deformation

As shown in the V displacement field in Figure 4(b) under the applied thermal loading, the module and the board bent into different curvatures in the x-y plane. Because of the unequal bending curvatures, the distance between the bottom surface of the module and the top surface of the board varies. The relative displacement of the two surfaces in the y direction is shown in Figure 5, where the index of solder ball n is used to label the horizontal axis. In this case (lowered temperature), all relative displacements are negative, implying that the two surfaces moved closer together everywhere. The relative displacement also describes the y-direction deformation of the solder joints because the solder height equals the distance between the

two surfaces. The nominal normal strain (y direction) in each solder joint can be calculated by dividing the relative displacement at that position (the centerline of the solder ball) by the height of the solder joints. The strain values are given in Figure 5 with the same curve but using the scale at the right-hand side, which was created by dividing the relative displacement value (the scale at the left-hand side) by the nominal solder height.

The solder strain shown in the figure is the total strain, which includes the following two parts: the thermal strain from a free thermal expansion of the solder and the mechanical strain from stress. The relation of these strains can be expressed as

$$\epsilon_{\text{total}} = \epsilon_{\text{mech}} + \alpha \Delta T,$$
 (3)

where  $\epsilon_{\rm mech}$  is the mechanical strain,  $\alpha$  is the CTE value, and  $\alpha \Delta T$  is the strain caused by the free thermal expansion.

The strain caused by the free thermal expansion can be obtained from the material properties. The free thermal expansion of the solder is 28 ppm/°C, which corresponds to -0.17% strain for a -60°C temperature change, shown as the horizontal dashed line in Figure 5. The mechanical strain is equal to the difference between the total strain (solid curve) and the free thermal expansion of the solder (dashed line). This is equivalent to shifting the curve so that the dashed line becomes the horizontal axis. As the assembly cools down to room temperature, the middle solder joints are subjected to slight compression and the two solder joints at each end (index  $n = \pm 8$  and  $\pm 9$ ) are subjected to tension of greater magnitude. Strain signs would be reversed if the temperature were increased. The deformation characteristic shown in Figure 5 is similar to the thermal deformation in the adhesive joint of a twolayer laminate described in [10]. This similarity is not surprising if we consider the solder ball array in an SBC package as a continuous layer of joint material between module and board.

# Macro shear deformation

Through use of the U field fringe pattern as shown in Figure 4(a), the relative displacement in the x direction between the two surfaces (the bottom surface of the module and the top surface of the board) can be determined. The resulting nominal shear strains in the solder joints can also be calculated (**Figure 6**). It is obvious that when the vertical centerline of the assembly is used as the reference point, the x-direction displacements as well as the shear strains should have opposite signs at the two sides of the assembly. In Figure 6, however, absolute values of the displacements and strains are used for simplicity. During the cooling process, the board shrank more than the module because of the CTE difference. Near the end of the module ( $n = \pm 9$ ), the board moved inward relative to the module by about 5  $\mu$ m. If the stress in the

solder joints were near zero because of solder relaxation, and the module and the board could deform freely during the temperature change, the relative shear displacement would be entirely dependent on the relative CTEs and would take the values given by the dashed lines. The difference in the two displacement curves (solid and dashed) is the result of the mechanical constraints that exist between the module and the board through the SBC joints, and the residual stresses in the solder joints. A similar situation exists when the package cools down from the elevated temperatures used in an assembly process; residual stresses remain in the solder joints and the structure.

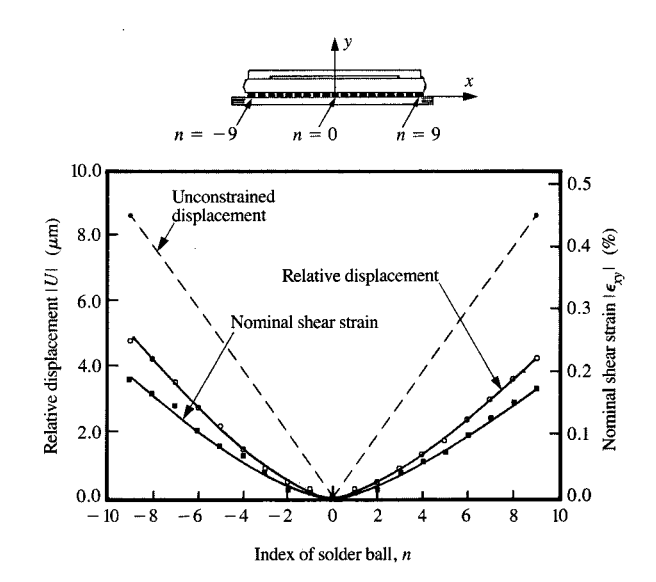
Because of the bending in the assembly (albeit small), the nominal shear strain in the solder joints cannot be calculated simply by dividing the relative shear displacement in the x direction by the nominal height of the solder joint, as was done when calculating the nominal normal strain. The nominal shear strain is obtained at the vertical centerline of each solder joint by combining the U and V displacement fields using the shear strain formula given in Equation (2). The maximum nominal shear strain occurs in the end solder joints where the macro DNP is the greatest. (DNP is the distance from the neutral point, which is generally located in the plane of symmetry.) Here, the macro DNP is defined as the DNP of the assembly, and the neutral point is located at the vertical centerline of the center solder joint. The shear strain values for the solder joints with lower macro DNPs are also given in Figure 6. Because free thermal expansion does not induce shear strain, the total shear strain in the solder joints is equal to the mechanical strain.

Similar shear strain distributions were found in the adhesive layer of a two-layer laminate [10] and in the encapsulated C-4 (Controlled Collapse Chip Connection) semiconductor packaging interconnections under thermal loading [9].

# • Micro deformations and strain concentrations in solder joints

The objective of the micromechanical analysis in this section is to determine the strain distributions and locations of strain concentrations within the individual solder joints and near the interfaces. Strain concentrations are usually localized in very small zones, and high spatial resolution is required to determine their magnitudes. In moiré interferometry, the spatial resolution can be increased by using a high-magnification imaging system when fringe patterns are recorded.

**Figure 7** shows high-magnification fringe patterns of the six rightmost solder joints (n = 4-9) of the cross section. [Figures 7(a) and 7(b) show the fringes from Figures 4(a) and 4(b) magnified.] Because of the CTE mismatch, high strains are developed in the solder near the interfaces with



Relative displacement between the module and the board in the x direction, and the nominal shear strain in each solder joint. The dashed line gives the relative x-direction displacement that would exist between the module and the board if the assembly were free of mechanical constraint from the solder joints. Absolute values are used in the plots for simplicity.

the module and the board. Strain concentrations are found at the "corners" of the solder joints.

The force components acting on the two interfaces, between the solder ball and the module and between the solder ball and the board, are schematically depicted in Figure 8. A simplification is used in depicting the cross section of the solder joint as a rectangular shape; the true shape was shown in Figure 2(c). These forces can be resolved into four components at each interface: (a) a uniform normal force, (b) a uniform shear force, (c) a moment which is equivalent to a distributed normal force, and (d) a distributed shear force. The uniform normal and shear forces are caused by the CTE mismatch between the module and the board (macro CTE mismatch), as is the case in most laminated structures. The distributed shear forces are caused by the micro CTE mismatches at the two connecting interfaces of the solder joint. The moments in (c) are the reacting forces from the module and the board to balance the shear forces in (b). The strains in the solder joints are the results of these forces, which vary from solder joint to solder joint.

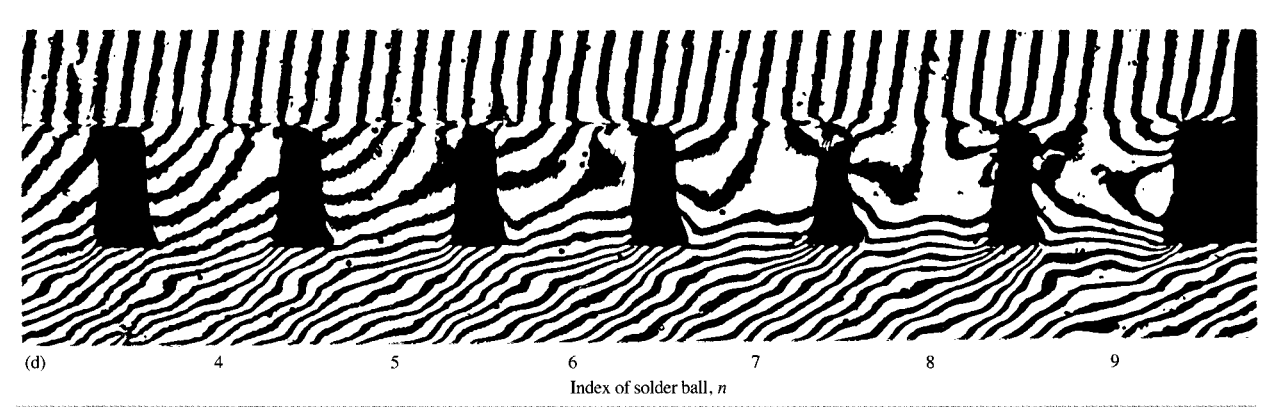
# Normal strains

Figure 7(d) is a V displacement fringe pattern showing the rightmost six solder joints of the cross section obtained by



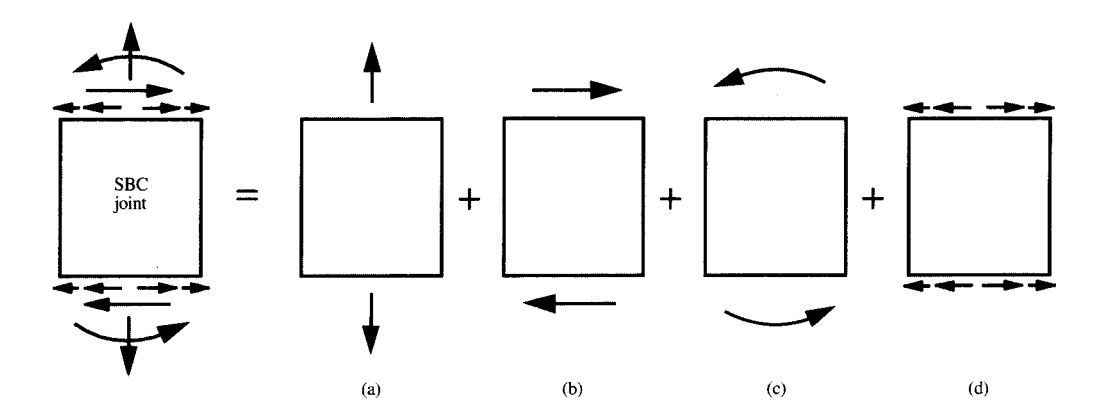






### Figure

Fringe patterns showing the micro effects at the rightmost six solder joints of the cross section. (a) original U displacement field; (b) original V displacement field; (c) U displacement field with carrier fringes added to cancel the rigid-body rotation at solder joint 4; (d) V displacement field with carrier fringes added to cancel the rigid-body rotation at solder joint 9.

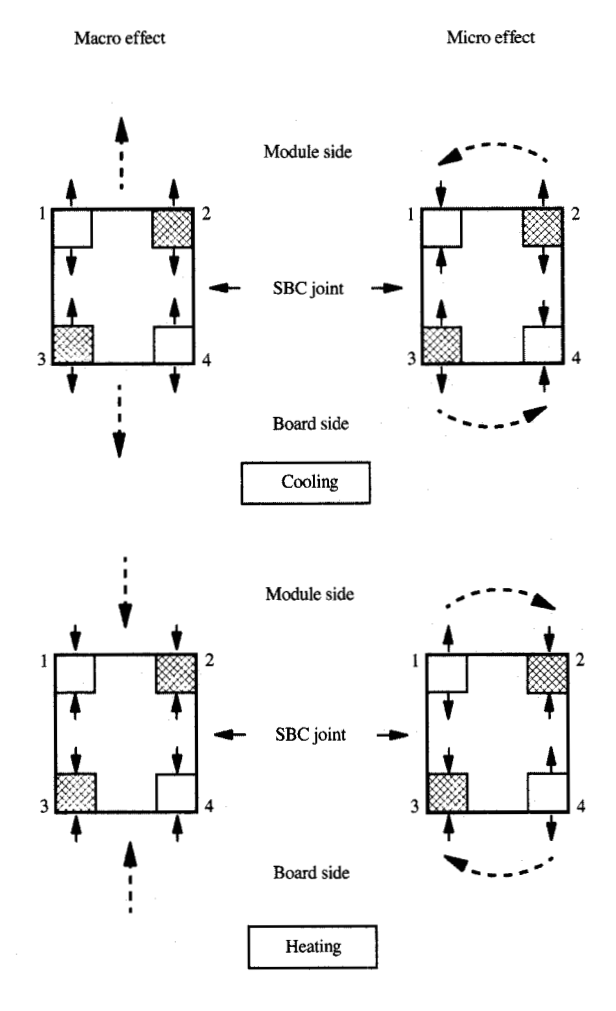


Forces acting on an SBC joint with a nonzero macro DNP: (a) uniform normal forces; (b) uniform shear forces; (c) moments; (d) distributed shear forces.

adding carrier fringes to the fringe pattern shown in Figure 7(b). The carrier fringes alter the fringe appearance but retain the original displacement information [7]. In Figure 7(d), the carrier fringes cancel the rigid-body rotation in the rightmost solder ball (n = 9), so that the normal strains in the v direction can be observed more easily. The high fringe gradients at the four corners of the solder joint clearly show normal strain concentrations. If the four corners of the solder joint are numbered 1, 2, 3, and 4 as in Figure 9, normal strains are found to be tensile at corners 2 and 3 and compressive at 1 and 4. This strain distribution is dictated by the interfacial forces shown in Figure 8. The forces acting on the interfaces of the rightmost solder ball are schematically described in Figure 9, where the forces represented by dashed arrows are the force components (the uniform normal forces and the moments) shown in Figure 8, and the forces represented by solid arrows are the resulting forces acting on small elements located at the four corners of the solder joint. The moment components create distributed normal forces, which have larger magnitudes near the edges of the interfaces; thus, the maximum effect is on one of the corner elements. The distribution of normal force is considered to be a micro effect because it is related to the solder joint geometry and its location. If the solder were a continuous layer or a one-dimensional thin rod, this micro effect would vanish.

During thermal cycles, the interfacial forces change signs and magnitudes and cause different strain distributions in the solder joints. However, the normal forces from the macro and micro effects always have the same sign at corners 2 and 3 (shaded areas) but opposite signs at corners 1 and 4, independent of whether the assembly is being heated or cooled. Thus, no matter how the temperature changes, the maximum normal strain always occurs at corners 2 and 3. When a cooling process takes place, the macro effect on the rightmost solder joint is uniform tension, according to the curve shown in Figure 5. The micro effect on the rightmost solder joint, a distributed force at the interfaces, causes tensile strain concentrations in corners 2 and 3 and compressive strain in corners 1 and 4. At corners 2 and 3, since the strains from macro and micro effects have the same sign, the superposition results in a larger total strain value. At corners 1 and 4, the strains cancel each other and result in a smaller total strain value. Since the result is temperatureindependent, it is obvious that during thermal cycles, corners 2 and 3 experience larger strain cycles and will be the locations most susceptible to fatigue failures.

In an individual solder joint, the micro effect has strong impact on the normal strain concentrations. For the particular solder joint geometry of the SBC sample used in this investigation, the nominal normal strain in the n=9 solder joint was approximately 0.1% (the mechanical strain shown in Figure 5). The maximum normal strain at corner 2, however, was about 0.5% [11], which means that there is a strong normal strain concentration. It also means that the normal strain varies dramatically in the solder joints. In this case, it would be a poor approximation to use the nominal strain (or average strain) to represent the solder strain. Since the strain concentration is closely related to features of the solder joint geometry (such as solder fillet



Macro and micro effects on the normal strain at the four corners of the rightmost solder joint.

shape and size), changing the joint shape can significantly reduce the maximum strain and improve the solder fatigue life.

A detailed analysis of normal strains is presented in Part II of this paper, by Choi et al. [11]. Whole-field strains and their numerical values are provided.

### Shear strains

The shear strains in each individual solder joint can be analyzed in the same way as the normal strains. The U displacement fringe pattern shown in Figure 7(c) was obtained by adding carrier fringes to the fringe pattern shown in Figure 7(a). The carrier fringes were used to cancel the nominal shear strain (the uniform part of the

shear strain) in the n = 4 solder joint (an arbitrary choice), so the resultant fringes show only the micro effect—the shear strain caused by the micro CTE mismatches at the interfaces. Similar to what was discussed in the section on macro shear deformation, the micro shear strain is a function of the local DNP (the DNP measured at the interfaces of an individual solder joint, with the neutral point at the axis of symmetry of the solder joint). At the interface region in a solder joint, the micro shear strain is zero at the center of the symmetry (the neutral point) and increases dramatically near the edges of the interface. When the fringe pattern of the n = 4 solder ball in Figure 7(c) is compared with the fringe pattern of the n=0solder ball in Figure 4(a), the one with no macro shear strain, it is clear that the micro effect has the same impact on both solder joints under a thermal load. In fact, since all the solder joints have the same nominal size and the same interface areas with the module and the board, the resulting shear strains from the micro effect should be identical in all of the solder joints, independent of their locations in the assembly. The shear strains caused by the micro effect (micro CTE mismatch) have the distribution characteristic typical of the shear strain at an interface between two materials with different mechanical properties, where the shear strain concentrations are localized only near the edges of the interfaces. If the solder were a continuous layer or a one-dimensional thin rod, as discussed in the section on normal strain, the micro effect of the shear strain would vanish as well.

The shear forces in the rightmost solder joint during a thermal cycle are schematically depicted in Figure 10, where the forces represented by dashed arrows are two shear force components described in Figure 8, and the forces represented by solid arrows are the resulting forces acting on the small elements located at the four corners of the solder joint. With respect to the x direction, under cooling, the solder joint contracts almost freely at the center but is constrained at the top and bottom interfaces where the micro CTE mismatches occur. The solder joints that have nonzero macro DNP also experience shear strains developed by the macro CTE mismatch, as shown in Figure 6. The resulting nominal shear strain in the solder balls due to this macro effect is a function of macro DNP. The total shear strain in each of those small elements is a sum of the shear strains from the macro and micro effect (Figure 10). The same effect of the signs of the forces discussed in the section on normal strains is also found in the shear forces. The shear forces in the rightmost joint from the macro and micro effects always have the same sign and are additive at corners 2 and 3 (shaded areas). They always have opposite signs and are subtractive at corners 1 and 4. Consequently, large shear strains are always located at corners 2 and 3 independent of heating or cooling in the thermal cycles. On the other

644

hand, corners 1 and 4 of the same solder joint always have smaller shear strains, no matter how the temperature changes.

As can be seen in Figure 7(a), there is a great difference in the shear strain values between corners 1 and 2 of the rightmost solder joint. For the conditions described above (a 25-mm SBC package with 0.89-mm solder balls under a temperature change of -60°C), in the rightmost solder joint and at the interface with the module, the shear strain concentration caused by the micro effect has a magnitude close to the nominal shear strain (0.18% as shown in Figure 6) caused by the macro effect. Consequently, at corner 1, by subtraction, the shear strain is small, and at corner 2, by addition, the shear strain reaches the maximum value (0.5%)—more than twice the nominal shear strain value. The numerical values of the shear strains and their distributions in the solder joints are presented in Part II of this paper, by Choi et al. [11].

# **Summary and conclusions**

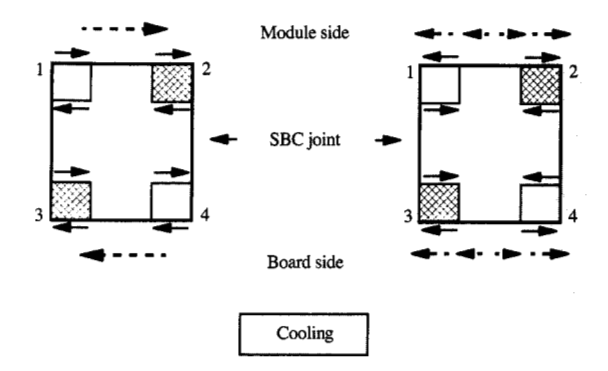
It has been found that the thermal deformations and the strain concentrations in SBC joints are the results of macro and micro effects in the package. The macro effect is caused by the CTE mismatch between the module and the board (the macro CTE mismatch), and the micro effect is due to the micro CTE mismatches and the local forces at the interfaces of the solder joint with the module and with the board.

The strain concentrations in an individual solder joint can be analyzed using the approach of macro and micro effect. For a given SBC package, the strain caused by the macro effect is a function of the macro CTE mismatch and the DNP. The strain concentrations caused by the micro effect are local effects, closely related to micro CTE mismatches and solder geometry. Through this approach, the strains in the SBC solder joints can be better understood, and improvements in designs can be carried out to reduce the strains.

There are strong normal and shear strain concentrations in the SBC solder joints, and strain variations are dramatic. The maximum normal strain is 0.5%, five times greater than the nominal normal strain, and the maximum shear strain is 0.5%, two times greater than the nominal shear strain. The strain concentrations are significant, and the values change substantially according to the joint geometry. On the other hand, the nominal strains have relatively small values and are insensitive to the solder joint geometry.

It is understood that when the nominal (average) shear strain is used as the effective strain to correlate the solder fatigue data, this strain must be the dominating strain which causes the fatigue damage in the solder. In SBC solder joints, the strain concentrations are significant, and the maximum strain is much greater than the nominal

Macro effect Micro effect



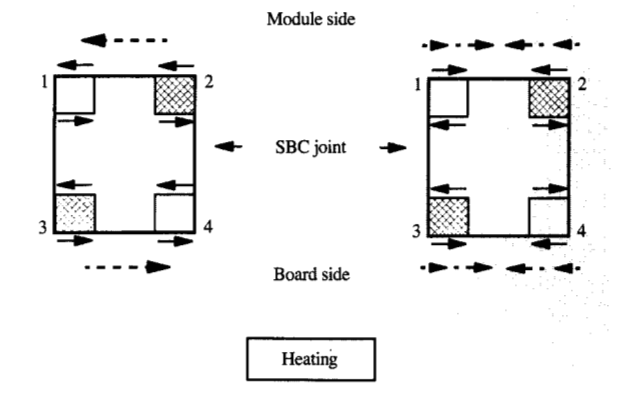


Figure 10

Macro and micro effects on the shear strain at the four corners of the rightmost solder joint.

strain. In this case, predictions of solder fatigue life using only the nominal strain may not be satisfactory.

Because the strain concentrations are closely related to solder geometry, it is very important to optimize the shapes of the solder joints under the given structural, electrical, and temperature constraints. It is a simple fact that any fillet with a sharp angle will have much higher strain concentrations than a fillet with a smooth curvature. Thus, changing the curvature of a solder fillet can dramatically reduce the strain concentrations. As a general design process, a verified finite element model offers a faster and more comprehensive optimization for different design parameters than do experimental evaluations, because it does not require hardware specimens. The finite

element model described by Corbin [12] was verified by the experimental results presented in this paper. In the IBM SBC program, this numerical model was used extensively to predict geometry and material sensitivities and to provide optimized parameters for general designs of SBC packages.

Fringe patterns from the experiment clearly indicated the sites of possible failure in the solder joints. Because of the high normal and shear strain concentrations, fatigue damage occurs first at corners 2 and 3 in the solder fillets during thermal cycles. Fatigue cracks are initiated there and propagate as plastic strains accumulate. The consequence is that the solder ball moves out of its original position as the crack propagates across the entire interface. The strain distributions and the failure modes described in this paper actually are common situations in surface mount packages using solder balls to connect two components with different CTEs. High strains and thermal fatigue damage in the solder joints always take place at corners 2 and 3. Corner 2 is the region of the interface between the solder ball and the component with the lower CTE that is farthest from the macro neutral point; corner 3 is the region of the interface with the component with the higher CTE that is closest to the macro neutral point.

It should be noted that deformation results obtained from a sectioned sample represent deformations at the surface of the cross section. In the analysis of macro deformations, cross-sectioning has little influence on the relative displacements between the module and the board, because cross-sectioning does not change the macro structure of the package. The values of the local strain concentrations in the SBC joints, however, are influenced by the cross-sectioning, which changes the local boundary conditions. On the surface of the cross section of a joint, the boundary condition is changed from displacement = 0to stress = 0. Nevertheless, this influence on the strain values is not greater than the change of the boundary condition from plane-strain to plane-stress. In addition, in this experimental study, the error caused by the cross-sectioning is no more significant than other variations involved in structural dimensions and materials properties. Therefore, the error caused by the crosssectioning was not extensively analyzed. For a more accurate analysis, a finite element model can be constructed to estimate the strain error caused by the cross-sectioning.

Moiré interferometry is a very powerful and effective tool for determining whole-field thermal strains and displacements. The experimental analysis of SBC packages provides an example of how this technique can be applied in the field of electronic packaging. By means of this technique, thermal strain distributions were determined for small solder joints, an analysis that could not be done experimentally in the past. The experimental results show

that moiré interferometry has great potential in future research and development of electronic packaging.

# **Acknowledgments**

The authors express their appreciation to T. Caulfield, for his significant support of this work and for the SBC photograph used in this paper, and to H.-C. Choi, B. Han, S. Merrill, and D. Strope, for their help in the experiments and in writing the paper.

### References

- K. C. Norris and A. H. Landzberg, "Reliability of Controlled Collapse Interconnections," *IBM J. Res. Develop.* 13, No. 3, 266-271 (May 1969).
- J. H. Lau and D. W. Rice, "Solder Joint Fatigue in Surface Mount Technology, State of the Art," Solid State Technol. 28, 91-104 (October 1985).
- P. M. Hall, "Force, Moment and Displacement During Thermal Chamber Cycle of Leadless Ceramic Chip Carrier Soldered to Printed Circuit Board," *IEEE Trans.* Components, Hybrids, Manuf. Technol. CHMT-7, No. 4, 314–327 (December 1984).
- T. D. Dudderar, N. Nir, A. R. Storm, and C. C. Wong, "Isothermal Low-cycle Fatigue Testing of Microscale Solder Interconnections," *Exper. Mechan.* 32, No. 1, 11–20 (March 1992).
- J. R. Wilcox, R. Subrahmanyan, and Che-Yu Li, "Thermal Stress Cycles and Inelastic Deformation in Solder Joints," Proceedings of the 2nd ASM International Electronic Materials and Processing Congress, Philadelphia, April 1989, pp. 203-211.
- D. Post, "Moiré Interferometry," Handbook on Experimental Mechanics, A. S. Kobayashi, Ed., Prentice-Hall, Inc., Englewood Cliffs, NJ, 1987, Ch. 7, pp. 314-387.
- Y. Guo, D. Post, and R. Czarnek, "The Magic of Carrier Patterns in Moiré Interferometry," Exper. Mechan. 29, No. 2, 169-173 (June 1989).
- 8. D. Post and J. Wood, "Determination of Thermal Strains by Moiré Interferometry," *Exper. Mechan.* 29, No. 3, 318-322 (September 1989).
- Y. Guo, W. Chen, and C. K. Lim, "Experimental Determinations of Thermal Strains in Semiconductor Packaging Using Moiré Interferometry," Proceedings of the ASME/ISME Joint Conference on Electronic Packaging, San Jose, CA, April 1992, pp. 779-784.
- W. T. Chen and C. W. Nelson, "Thermal Stress in Bonded Joints," IBM J. Res. Develop. 23, No. 2, 179-180 (March 1979).
- H.-C. Choi, Y. Guo, W. LaFontaine, and C. K. Lim, "Solder Ball Connect (SBC) Assemblies Under Thermal Loading: II. Strain Analysis via Image Processing, and Reliability Considerations," IBM J. Res. Develop. 37, No. 5, 649-659 (1993, this issue).
- J. S. Corbin, "Finite Element Analysis for Solder Ball Connect (SBC) Structural Design Optimization," IBM J. Res. Develop. 37, No. 5, 585-596 (1993, this issue).

Received January 6, 1993; accepted for publication August 9, 1993

Yifan Guo IBM Microelectronics Division, 1701 North Street, Endicott, New York 13760 (YIFAN at ENDVMTKL, yifan@endvmtkl.vnet.ibm.com). Dr. Guo received his Ph.D. degree in engineering mechanics from Virginia Polytechnic Institute and State University in 1989. After graduation, he was appointed as Assistant Professor in the Engineering Science and Mechanics Department at VPI&SU. He taught courses in mechanics and continued his research in the area of experimental mechanics and mechanics of composite materials. Dr. Guo joined IBM in 1990 as a Staff Engineer and began his research in the field of microelectronic packaging using laser interferometry and other experimental techniques. He recently received an IBM Division Award for his contributions in the development and applications of moiré interferometry in electronic packaging.

Chun K. Lim IBM Microelectronics Division, 1701 North Street, Endicott, New York 13760 (LIMCKL at ENDVMTKL, limckl@endvmtkl.vnet.ibm.com). Dr. Lim is a Senior Technical Staff Member and Manager of Metallurgy and Micromechanics. He received the B.S. degree in mechanical engineering from the University of Missouri and the Ph.D. in engineering science and mechanics from Pennsylvania State University. He held a postdoctoral fellowship in materials science at the California Institute of Technology. Dr. Lim is a member of the Society of Experimental Mechanics, the American Society of Mechanical Engineers, and the Korean Scientists and Engineers Association in America. His current interests are materials and mechanics issues in microelectronics packaging. He has received an IBM Outstanding Innovation Award, an IBM Outstanding Contribution Award, an IBM President's Award, and the 4th Level Publications Achievement Award.

William T. Chen IBM Microelectronics Division, 1701
North Street, Endicott, New York 13760 (CHENWT at
ENDVMTKL, chenwt@endvmtkl). Dr. Chen received a B.S.
degree in mechanical engineering from Queen Mary College,
London University; an M.S. from Brown University; and a
Ph.D. from Cornell University in theoretical and applied
mechanics. He joined IBM in 1963. Dr. Chen has been
active in various aspects of electronic packaging product
development and manufacturing, including design, materials,
processes, and reliability. His interest has been in applying
knowledge of mechanics, materials, and physics to engineering
practices of design and manufacturing for leading-edge
electronic packaging products. Dr. Chen is a Fellow of the
American Society of Mechanical Engineers; he has been
elected to the IBM Academy of Technology.

Charles G. Woychik IBM Microelectronics Division, 1701 North Street, Endicott, New York 13760 (WOYCHIK at ENDVMTKL). Dr. Woychik received his Ph.D. from Carnegie-Mellon University in materials science in 1984. He is currently a manager in the Assembly Process Design organization in Endicott. He has received five patents and attained the second level of invention award in IBM. He has published papers on the subject of electronic materials, particularly those related to solder alloy development and transient liquid-phase bonding. Dr. Woychik teaches internal and external classes on the subject of electronic packaging-assembly processes. Currently, he is involved in developing new assembly processes that are environmentally safe and more cost-effective than current processes.

